THE JOURNAL OF BIOLOGICAL CHEMISTRY VOL. 289, NO. 37, pp. 25590–25600, September 12, 2014

Phototransformation of the Red Light Sensor Cyanobacterial Phytochrome 2 from *Synechocystis* Species Depends on Its Tongue Motifs*

Received for publication, March 3, 2014, and in revised form, July 3, 2014 Published, JBC Papers in Press, July 10, 2014, DOI 10.1074/jbc.M114.562082

Katrin Anders[‡1], **Alexander Gutt**[§1,2], **Wolfgang Gärtner**[§2,3], **and Lars-Oliver Essen**[‡4]

From the [‡]*Departments of Chemistry and Biology, Philipps-University, D-35032 Marburg and the* [§]*Max-Planck Institute for Chemical Energy Conversion, D-45470 Mülheim a. d. Ruhr, Germany*

Background: Phytochromes are bilin-dependent red/far red photoreceptors.
Results: Late processes of the $P_r \rightarrow P_{fr}$ photoconversion involve large scale conformational changes within the tongue region.
Conclusion: Early intermediates lumi-R and R1 affect only the chromophore and its nearest surroundings, whereas late R2 formation recruits the Trp motifs in the peripheral tongue.
Significance: The conserved motifs of the tongue region are important for photoconversion and presumably for signaling.

Phytochromes are photoreceptors using a bilin tetrapyrrole as chromophore, which switch in canonical phytochromes between red (P_r) and far red (P_{fr}) light-absorbing states. Cph2 from *Synechocystis* sp., a noncanonical phytochrome, harbors besides a cyanobacteriochrome domain a second photosensory module, a P_r/P_{fr}-interconverting GAF-GAF bidomain (*Syn*Cph2(1-2)). As in the canonical phytochromes, a unique motif of the second GAF domain, the tongue region, seals the bilin-binding site in the GAF1 domain from solvent access. Time-resolved spectroscopy of the *Syn*Cph2(1-2) module shows four intermediates during $P_r \rightarrow P_{fr}$ phototransformation and three intermediates during $P_{fr} \rightarrow P_r$ back-conversion. A mutation in the tongue's conserved PR*X*SF motif, S385A, affects the formation of late intermediate R3 and of a P_{fr}-like state but not the back-conversion to P_r via a lumi-F-like state. In contrast, a mutation in the likewise conserved W*X*E motif, W389A, changes the photocycle at intermediate R2 and causes an alternative red light-adapted state. Here, back-conversion to P_r proceeds via intermediates differing from *Syn*Cph2(1-2). Replacement of this tryptophan that is ~15 Å distant from the chromophore by another aromatic amino acid, W389F, restores native $P_r \rightarrow P_{fr}$ phototransformation. These results indicate large scale conformational changes within the tongue region of GAF2 during the final processes of phototransformation. We propose that in early intermediates only the chromophore and its nearest surroundings are altered, whereas late changes during R2 formation depend on the distant W*X*E motifs of the tongue region. Ser-385 within the PR*X*SF motif affects only late intermediate R3, when refolding of the tongue and docking to the GAF1 domain are almost completed.

Within the broad range of photoreceptors existing in photosynthetic and nonphotosynthetic bacteria, bilin-binding GAF domain-containing proteins like phytochromes and cyanobacteriochromes (CBCRs)[5] cover the whole light spectrum. Despite different spectral characteristics between the red/far red-light absorbing phytochromes and CBCRs, which switch between all kinds of colors, they both harbor the same kind of chromophore, a covalently attached linear tetrapyrrole. Classical phytochromes photoconvert between two conformations, the red and far red light-absorbing P_r and P_{fr} state. Upon red light illumination of P_r, the excited state P_r^* is formed, which decays and converts into the primary red-shifted photoproduct lumi-R (also called I_{700}) within picoseconds (1). This step involves the $Z \rightarrow E$ isomerization of the C15, C16 double bond of the bilin chromophore. The further steps are light-independent and proceed thermally driven in longer time scales. Accordingly, phytochrome photoconversion starts within picoseconds and can last up to seconds (2, 3). The light-triggered reaction from $P_{fr} \rightarrow P_r$ undergoes different intermediates (4, 5).

Full-length oat PhyA shows pairs of intermediates in the $P_r \rightarrow P_{fr}$ phototransformation with similar spectroscopic signatures but different lifetimes (2). This is caused by at least two distinct P_r conformations each leading to one set of subsequent intermediates (6). Cph1 from *Synechocystis* sp., a bacterial phytochrome commonly used as a model for plant phytochromes, exhibits a multistep photoconversion reminiscent of the PhyA $P_r \rightarrow P_{fr}$ reaction. However, *Syn*Cph1 displays a different kinetics (5, 7) with an intermediate that has no counterpart in any other phytochrome.

* This work was supported in part by Deutsche Forschungsgemeinschaft Grants ES152/9 and ES152/10.
[1] These authors contributed equally to this work.
[2] Recipient of support from the Max-Planck Society.
[3] To whom correspondence may be addressed: Max-Planck Institute for Chemical Energy Conversion, Stiftstrasse 34-36, D-45470 Mülheim a. d. Ruhr, Germany. Tel.: 49-208-306-3693; E-mail: wolfgang.gaertner@cec.mpg.de.
[4] To whom correspondence may be addressed: Dept. of Chemistry, Philipps-University Marburg, Hans-Meerwein-Str. 4, D-35032 Marburg, Germany. Tel.: 49-6421-28-22032; Fax: 49-6421-28-22191; E-mail: essen@chemie.uni-marburg.de.

[5] The abbreviations used are: CBCR, cyanobacteriochrome; GAF, cGMP phosphodiesterase/adenylyl cyclase/FhlA; PCB, phycocyanobilin; PAS, period/ARNT/single-minded; PHY, phytochrome; LADS, lifetime-associated difference spectra.

In contrast to canonical phytochromes from plants or bacteria, the domain architecture of the second phytochrome from *Synechocystis* sp., *Syn*Cph2, exhibits some remarkable differences. First of all, *Syn*Cph2 is a bimodule photoreceptor (~145 kDa) with a complex domain architecture, GAF1-GAF2-GGDEF1*-EAL-GAF3-GGDEF2 (8, 9). The common PAS-GAF-PHY sensor module (PAS (Period/ARNT/Single-minded), GAF (cGMP phosphodiesterase/adenylyl cyclase/FhlA), and PHY (phytochrome)), which defines canonical group I phytochromes (10), is here altered to a GAF-GAF bidomain (group II phytochromes) as the N-terminal photosensory module. This *Syn*Cph2(1-2) module exhibits P_r/P_{fr} photochromicity known from group I phytochromes (9), where the PHY domain has been structurally recognized as a GAF domain as well (11). *Syn*Cph2 covalently attaches phycocyanobilin (PCB) via a thioether linkage that is partly solvent-exposed due to the missing PAS domain (8). Similar to plant phytochrome B, but unlike *Syn*Cph1 and PhyA, the P_{fr} state of this photosensory module undergoes dark reversion to its P_r state (9). Besides the UV-visible spectra, resonance Raman spectra of *Syn*Cph2(1-2), which are highly sensitive to structural changes at the chromophore-binding site, resemble closely the spectral features of *Syn*Cph1 in both states, P_r and P_{fr}. Given the lack of a PAS domain, one may consider the *Syn*Cph2(1-2) module as a minimal model of P_r/P_{fr} photoconversion in canonical phytochromes. Besides the red/far red light-sensitive GAF-GAF bidomain, *Syn*Cph2 harbors a CBCR-like GAF3 domain as its second photosensory module with a blue/green photochemistry. This photochromic switch controls light-regulated cyclic di-GMP levels (12) by tuning the catalytic activity of the GGDEF2 domain. GGDEF and EAL domains (named after their conserved motifs) produce and degrade, respectively, cyclic di-GMP, a eubacterial second messenger (13). A GGDEF1*-EAL module with an inactive GGDEF domain is found in *Syn*Cph2 following the N-terminal GAF bidomain sensor module (Fig. 1*A*).

The crystal structure (8) of the red/far red phytochrome region confirmed that the GAF2 domain is directly related to the PHY domains of canonical phytochromes. Like the latter, it includes a tongue-like extension that covers the bilin-binding site of the GAF1 domain and may hence be involved in intramolecular signal transduction. Despite significant sequence divergence between the core GAF2 and PHY domains, three motifs within the tongue region, W(G/A)G, PR*X*SF, and W*X*E, are almost invariant in group I and II phytochromes and were hence suggested to be crucial for phototransformation and stability of the resulting P_{fr} state. The significance of the bulky aromatic character of the tryptophan residues in the W(G/A)G and W*X*E motifs for P_{fr} formation was derived from site-directed mutagenesis and structural comparison with the tongue conformation of bathyphytochromes in their P_{fr} ground state (8). The resulting model of a "tryptophan switch" during photoconversion implies that the tongue undergoes a red light-triggered conformational change thus altering the conformation and/or orientation of the conserved PR*X*SF motif and thereby its interactions with the chromophore-binding site. In this context, the tryptophans of the W(G/A)G and W*X*E motifs are supposed to swap their positions and play an important role in the stabilization of a P_{fr}-specific conformation of the tongue region (8). This model was recently corroborated by the findings in *Deinococcus radiodurans* phytochrome that shows the predicted features of the tryptophan switch model by the structures of its P_r and P_{fr} states (14).

Here, we characterize *Syn*Cph2(1-2) and three of its tongue mutants by time-resolved absorption spectroscopy to track slow conformational changes, which are mostly indicative of structural changes within the protein moiety. Whereas the native *Syn*Cph2(1-2) module and its W389F mutant exhibit both a cognate spectral behavior under steady state conditions, the W389A and S385A mutants were found to fail in the formation of a P_{fr}-like state upon red light illumination (Fig. 1*B*). We analyzed the light-induced $P_r \rightarrow P_{fr}$ and $P_{fr} \rightarrow P_r$ photoconversions in the micro- to millisecond time range by laser flash photolysis and time-resolved absorption spectroscopy. The data were used in global fit analysis to obtain lifetime-associated difference spectra (LADS) of the intermediates.

MATERIALS AND METHODS

*Syn*Cph2(1-2) and mutants were produced and purified as described (9); the measurements with the PCB-assembled proteins were performed in Tris buffer (50 mM Tris, 300 mM NaCl, 5 mM EDTA, pH 8.0). For flash photolysis, the protein sample was diluted to an absorbance of 0.5 at the P_r maximum using a cuvette of a 1-cm path length. Absorption spectra were recorded before and after the measurements (spectrophotometer UV-2401 P, Shimadzu) to exclude denaturation of the protein. The sample was kept in a quartz cuvette with a 1-cm path length was kept at 288 K (15 °C). Photoconversion of the proteins to 100% P_r or the highest P_{fr} occupancy was accomplished by irradiation with a 720 and a 625 nm LED light source (high power LED, Roithner; 720 nm, 350 mA; 1.8 V; 625 nm, 350 mA, 2.2 V), respectively. An optical parametric oscillator, coupled to a Spitlight 300 Ne-YAG laser (Versascon HB, GWU-Lasertechnik), was used for excitation (pulse length, 9 ns; energy output 640 nm, 70 μJ; 700 nm, 45 μJ) with $\lambda_{ex} = 640$ nm for the $P_r \rightarrow P_{fr}$ conversion and $\lambda_{ex} = 700$ nm for the reverse reaction. The resulting absorption changes were detected at various wavelengths between 520 and 720 nm. For *Syn*Cph2(1-2), the S385A and W389A mutant, the entire spectral range was recorded in 10-nm steps. The variant W389F was measured with seven wavelengths (590, 640, 660, 665, 690, 700, and 720 nm) that display the highest absorbance changes throughout the intermediate spectra, allowing the prediction of the photocycle according to the previously recorded spectra and lifetimes. Absorbance changes were detected via a continuous wave xenon lamp (Amko) and two matched monochromators (A 1020) placed before and behind the sample. Absorbance changes were recorded by a photomultiplier mounted to the second monochromator, from which the signals were read into a computer for further data handling and fitting. The detection range covered times between a few microseconds to 100 ms. The resolution is limited to ~0.1 μs at the lower time limit and ~1 μs at the higher time limit. Beyond 80 ms, the photoconversion was complete for *Syn*Cph2(1-2) as well as for its mutants. For each wavelength and single time traces, 10 measurements were averaged to improve the signal to noise ratio. Between individual measurements, the sam-

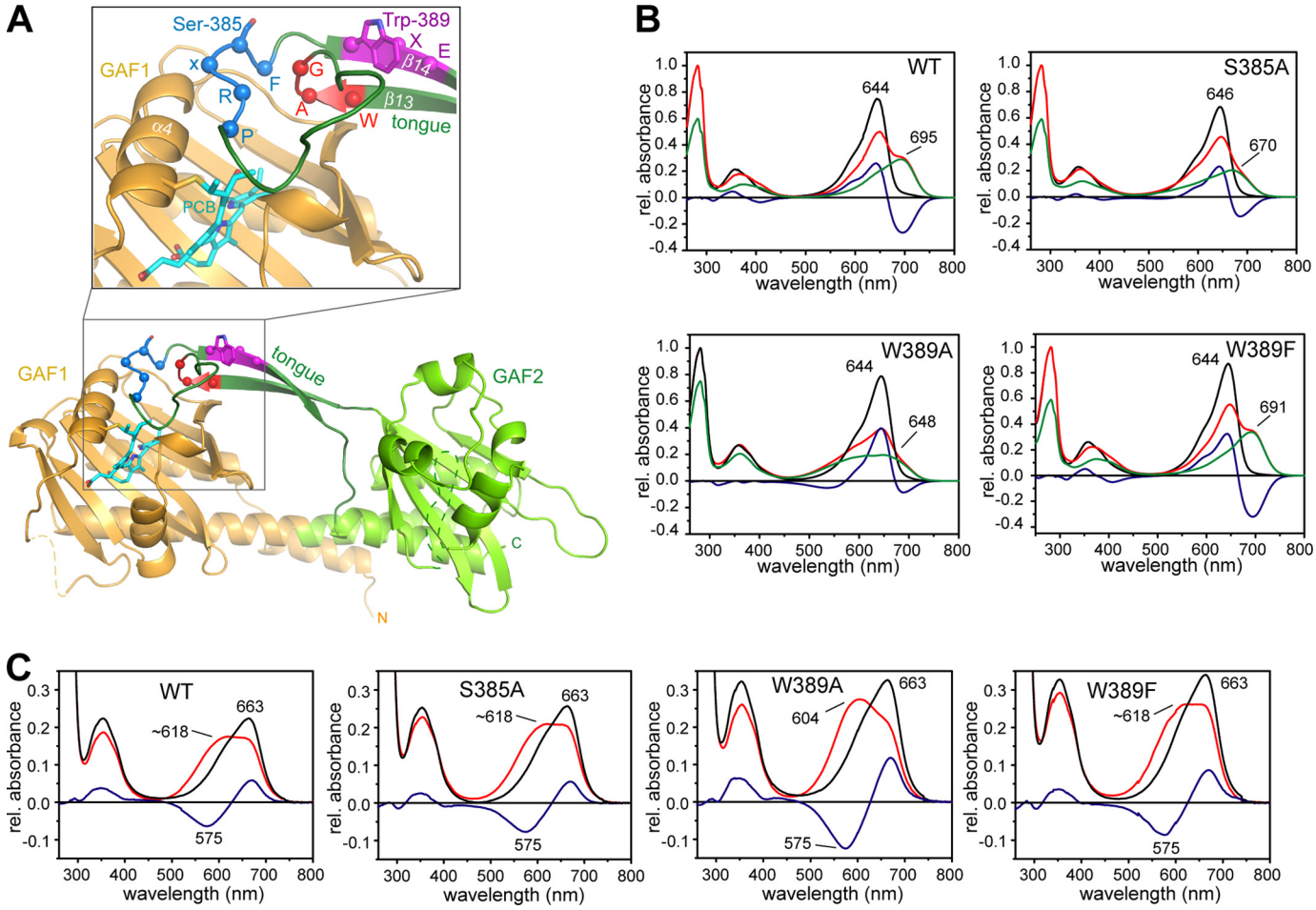

FIGURE 1. **Structure of *Syn*Cph2(1-2) (Protein Data Bank code 4BWI), including the positions of the mutations in the tongue region and absorbance of UV-visible spectra of the variants.** *A,* structure of *Syn*Cph2(1-2) with a detailed view of the chromophore binding pocket (*inlay*). The GAF1 domain is displayed in *orange*, and the GAF2 domain with the tongue region is displayed in *green*, respectively. The PCB chromophore is shown in *cyan*. Amino acid positions Ser-385 and Trp-389 as well as the cofactor binding Cys-129 are displayed in *stick* representation. The residues of the conserved W(G/A)G, PR*X*SF, and W*X*E motifs are depicted as *spheres*, and the motifs are highlighted in *red, blue,* and *magenta*, respectively. *B,* steady state UV-visible absorbance spectra of *Syn*Cph2(1-2) and the variants S385A, W389A, and W389F as shown in Ref. 8 after far-red (P_r state, *black line*) and red light illumination (*red line*). Difference spectra are calculated with $A_{Pr} - A_{Photoequilibrium}$ and shown in *blue*. Deconvoluted, pure P_{fr} (or red light-adapted) spectra are presented in *green* (9). At the photoequilibrium, a portion of 59% P_{fr}-like state for S385A, 75% P_{alt} for W389A, and 59% P_{fr} state for W389F are obtained in comparison with *Syn*Cph2(1-2) (60% (9)). *C,* UV-visible absorbance spectra of *Syn*Cph2(1-2) as well as S385A, W389A, and W389F after denaturation with acidic urea (denatured P_r state, *black line*; denatured red light-adapted state, *red line*; difference spectrum, *blue line*).

ple was irradiated with the LED light sources for 8 and 5 s, respectively, to revert photochemically generated products and to achieve maximal P_r or P_{fr} state occupancy.

For data analysis, the single time traces were baseline-corrected if necessary and assembled (usually three time windows with different scaling were measured separately and later combined into a single wavelength recording trace). Global fit analysis was performed by fitting the curves with a sum of exponential functions (MATLAB) (15–17), yielding lifetimes for the individual transitions between intermediates and the lifetime-associated difference spectra (LADS). Care was taken to minimize laser or scattering light artifacts during the short time windows that might impair detection of early intermediates. Derived lifetimes have a variance of about ±10% and do not influence selectively one or the other's lifetime. A more detailed study on canonical phytochromes (CphA) considers variations between consecutive measurements, temperature effects, and accumulation problems such as continuous back-irradiation or back-irradiation after one set of 3–5 single laser shots (18).

The acid denaturation assay was performed by addition of 8 M urea/HCl, pH 2, to a preliminarily irradiated protein sample in the dark at room temperature (19); subsequently, absorption spectra were recorded.

RESULTS

We hereby report the first kinetic study of the late intermediates of the $P_r \rightarrow P_{fr}$ phototransformation and the $P_{fr} \rightarrow P_r$ back reaction of a Cph2-type phytochrome module. We also address the influence of the highly conserved PR*X*SF and W*X*E motifs within the tongue on photoconversion. For that purpose, the S385A, W389A, and W389F mutants (Fig. 1*A*) were generated, and their chronology of intermediate formation during photoconversion was studied by time-resolved spectroscopy. In *Syn*Cph2(1-2) as well as in the mutant phototransformation was complete within 80 ms, and later intermediates could not be observed. The primary photochemical event, the $Z \rightarrow E$ photoconversion, is shared by *Syn*Cph2(1-2) as well as by the variants S385A, W389A, and W389F as proven by an acid

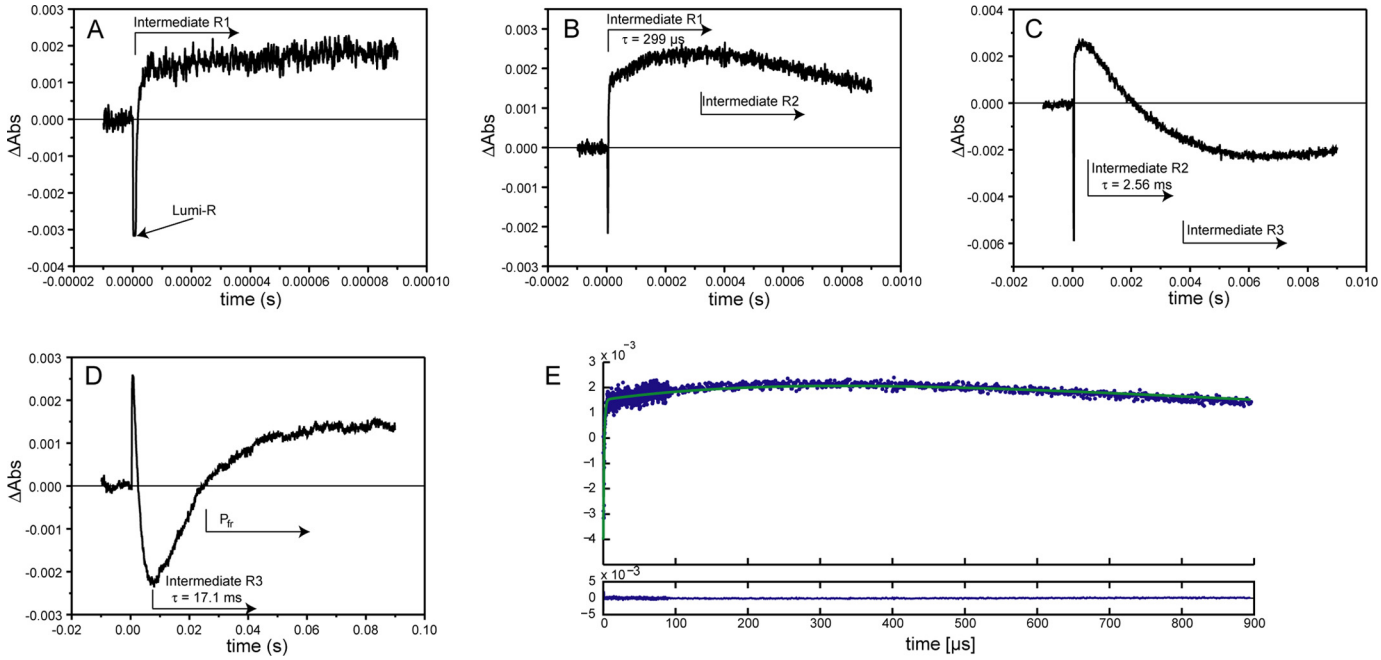

FIGURE 2. **Single time traces of the *Syn*Cph2(1-2) $P_r \rightarrow P_{fr}$ transition measured at 665 nm.** Here, the intermediates show alternately lower or higher absorbance than the P_r reference state and can be observed without further data analysis. *A–D* show the time traces with increasing time scales; the approximate appearance of intermediates is indicated by *arrows*. The intermediate lifetimes are also presented. The final intermediate R3 exhibits similar absorption as the P_{fr} conformation (*D*). The initial 10% of the time traces prior to the laser pulse are recorded to determine the baseline level; at $t = 0$ the laser flash triggered the photoconversion. *E*, individual time traces (*A–D*) were assembled. Here, the fit of the resulting data is shown in *green* as well as the residuals (below).

denaturation assay (19) of the P_r and red light-adapted state. Denatured P_r states show absorbance maxima at 663 nm like other PCB-cysteine adducts with 15*Z* conformation (19, 20). The denatured red light-adapted states show a mixture of the 15*Z* and 15*E* states (Fig. 1*C*). Here, the 15*E* state absorbance maximum at ~604 nm corresponds to other PCB-15*E* states as in *Syn*Cph1 (21).

Photokinetics of the SynCph2(1-2) Module—The $P_r \rightarrow P_{fr}$ transition was triggered by a 9-ns laser pulse of red light (λ = 640 nm) that was tuned close to the λ_{max} of the P_r state of *Syn*Cph2(1-2) (λ_{max} = 644 nm). During photoconversion, *Syn*Cph2(1-2) forms distinct intermediates that can all be followed in single time traces at 665 nm (Fig. 2). The formation of the first intermediate, lumi-R, occurs in phytochromes in the picosecond time range (1) and is hence too fast to be resolved in this study. Accordingly, the decay of a lumi-R-like state (lumi-R_L) represents the first observable process. For *Syn*Cph2(1-2) four intermediates, lumi-R_L, -R1, -R2, and -R3, were found for the $P_r \rightarrow P_{fr}$ conversion with lifetimes of 1.3 μs, 299 μs, 2.56 ms, and 17.1 ms (Table 1). Their spectral features are reflected by their LADS shown in Fig. 3. Notably, these LADS are defined as difference spectra, where positive amplitudes indicate a decaying species, *i.e.* the absorbance at the specific wavelength decreases between the preceding state and the observed one, whereas negative LADS amplitudes specify an absorbance rise.

During $P_r \rightarrow P_{fr}$ phototransformation of *Syn*Cph2(1-2), the first intermediate corresponds to the lumi-R-like state with an increase in absorbance at about 670 nm and a calculated lifetime of 1.3 μs. The bathochromic shift of the lumi-R_L absorbance as compared with the initial P_r state is continued by the next intermediate, R1 (lifetime 299 μs), due to a further rise of absorbance at 690 nm. The LADS of the R1 intermediate is bimodal as it shows also a shallow decrease of absorbance at 620 nm. Furthermore, its absorbance changes related to this lifetime show relatively small positive and negative amplitudes. The third intermediate, R2 (lifetime of 2.56 ms), reveals an absorbance decay at 660 nm thus further lowering the absorbance at shorter wavelengths. The last intermediate, R3 (lifetime of 17.1 ms), displays an absorbance rise already close to the P_{fr} maximum and thus is indicative for the dominant component of the final P_{fr} state formation. The resulting "constant," *i.e.* the difference spectrum between the initial and the final absorbances detected by the time-resolved measurements (Fig. 3, *green traces*), is very similar to the observed steady state difference spectrum (Fig. 1*B*) and therefore proves the applicability of the method.

For the $P_{fr} \rightarrow P_r$ transition (excitation at 700 nm), the global analysis revealed three intermediates (lumi-F, F1, and F2) with

TABLE 1

Intermediate lifetimes of *Syn*Cph2(1-2), S385A, W389A, and W389F photocycles

The lifetimes of *Syn*Cph2(1-2), S385A, and W389A are calculated via global fit analysis. The lifetimes of W389F are averages from fits of single time traces. The lifetimes of the first two intermediates of the $P_{fr} \rightarrow P_r$ photoconversion of W389F could not be derived (NA means not available) due to the low absorbance changes between its early intermediates.

	Wild type	S385A	W389A	W389F
P_r to P_{fr}				
Lumi-R	1.3 μs	1.3 μs	1.4 μs	1.5 μs
-R1	299 μs	112 μs	414 μs	380 μs
-R2	2.56 ms	1.57 ms	2.28 ms	2.0 ms
-R3	17.1 ms	8.10 ms		33.3 ms
P_{fr} to P_r				
Lumi-F	0.9 μs	1.3 μs	1.2 μs	NA
-F1	798 μs	619 μs	2.21 ms	NA
-F2	6.20 ms	3.53 ms	19.5 ms	3.1 ms

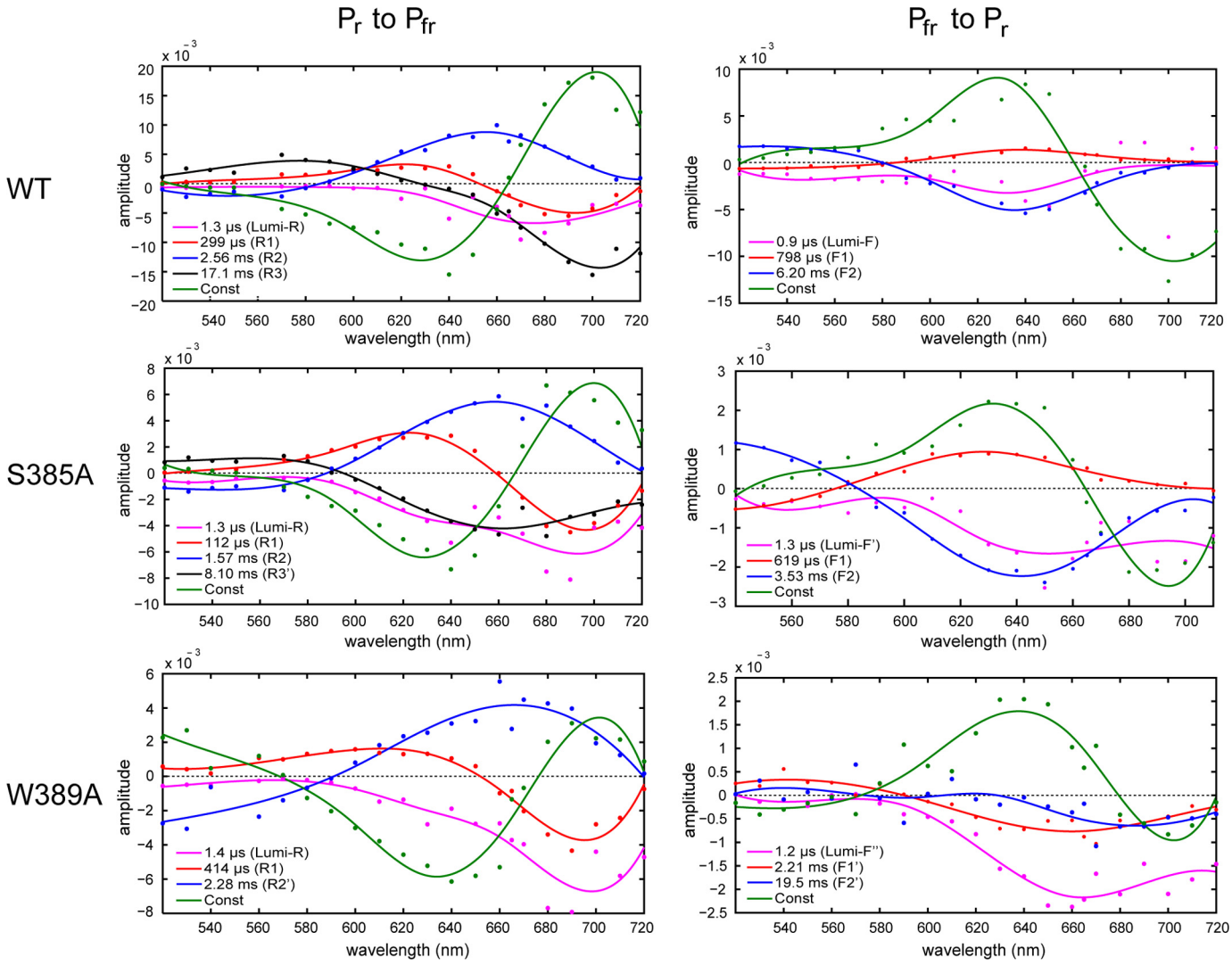

FIGURE 3. **LADS of *Syn*Cph2(1-2) (*top panel*) and its S385A (*middle*) and W389A variant (*bottom*) in the respective $P_r \rightarrow P_{fr}$ (*left*) or $P_{fr} \rightarrow P_r$ (*right*) transition.** The lifetimes of the intermediates are shown in the inlays. The constant difference spectrum (*green*) reflects the subtraction of the starting state absorbance spectrum from the final state that should correspond to the difference between P_r and P_{fr} ($P_r \rightarrow P_{fr}$ transition: $\Delta A = A(P_{fr}) - A(P_r)$). The other LADS show the subtraction of the intermediate spectrum from the previous intermediate spectrum ($P_r \rightarrow P_{fr}$ transition: $\Delta A = A(\text{Intermediate1}) - A(\text{Intermediate2})$). A positive absorbance difference in the LADS reflects an absorbance decay from the last to the considered intermediate, a negative signal of an absorbance increase.

lifetimes of 0.9 μs, 798 μs, and 6.20 ms. This makes the reverse photoconversion about three times faster than the $P_r \rightarrow P_{fr}$ phototransformation. Like other phytochromes, *Syn*Cph2(1-2) undergoes different intermediates than during the "forward" $P_r \rightarrow P_{fr}$ conversion. The absorbance changes between the intermediates are not as pronounced as in the $P_r \rightarrow P_{fr}$ phototransformation (Fig. 4), which is reflected in the LADS by displaying only small changes for the associated amplitudes (Fig. 3). Already the early lumi-F intermediate formed in the $P_{fr} \rightarrow P_r$ phototransformation resembles the P_r state, and the further F1 and F2 intermediates show only modest absorption changes. The last intermediate, F2, with a lifetime of 6.20 ms, displays an absorbance rise at about 640 nm and leads finally to the P_r state.

Light-induced Kinetics of SynCph2(1-2) Tongue Mutants—Ser-385 is located in the conserved PR*X*SF motif that is situated in the common tongue region of group I and II phytochromes. In the *Syn*Cph2(1-2) P_r crystal structure (8), this polar residue shows no interaction with the GAF1 domain and its embedded PCB chromophore and points away from the chromophore binding pocket, whereas in bathyphytochromes and the P_{fr} state of *D. radiodurans* phytochrome (14), this residue was found to form a hydrogen bond with the aspartate of the conserved DIP motif within the chromophore-binding site. Accordingly, the S385A mutant of *Syn*Cph2(1-2) exhibits a P_{fr} steady state absorbance spectrum that deviates significantly from that of the native *Syn*Cph2(1-2) module (Fig. 1*B*). After red light illumination of the P_r state, the P_{fr} spectrum shows a broadened peak in the red region between 500 and 620 nm. At the photodynamic equilibrium, the resulting spectrum exhibits a bleaching at 646 nm and an isosbestic point at 556 nm relative to the P_r state with its λ_{max} at 646 nm. At wavelengths shorter than the isosbestic point, the mutant shows increased absorbance upon photoconversion unlike native *Syn*Cph2(1-2).

The global analysis of the time-resolved data from the S385A mutant reveals, as in the native *Syn*Cph2(1-2), four intermedi-

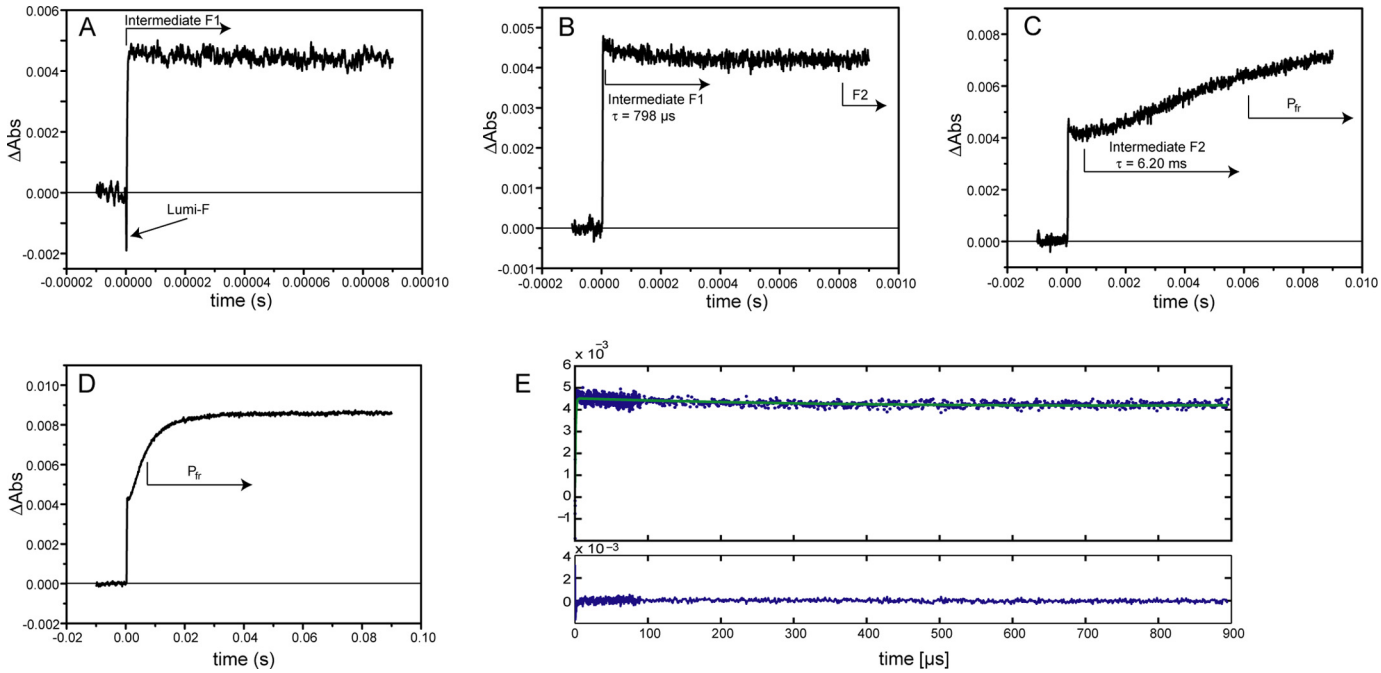

FIGURE 4. **Single time traces of the *Syn*Cph2(1-2) $P_{fr} \rightarrow P_r$ transition measured at 640 nm.** The absorbance difference between the intermediates is not as high as in the forward reaction. *A–D,* single time traces with increasing time scales are shown as well as the assignment of the absorbance differences to the intermediates and their lifetimes. As in the forward reaction, the formation of the first intermediate lumi-F is too fast for the resolution of these measurements. *E,* fit of the assembled data from *A* to *D* (*green*) and its residuals.

ates (lumi-R_L, R1, R2, and R3′) with lifetimes of 1.3 μs, 112 μs, 1.57 ms, and 8.10 ms for the forward reaction, *i.e.* $P_r \rightarrow P_{fr}$. The first three intermediates are similar to *Syn*Cph2(1-2) but with up to 3-fold shorter lifetimes. Accordingly, the overall photoconversion is about two times faster than in native *Syn*Cph2(1-2) and leads to a final state with a difference spectrum akin that of native *Syn*Cph2(1-2), but with a 2.6-fold reduced overall amplitude. Likewise, the late R2 and R3 intermediates exhibit similarly lowered overall amplitudes, whereas the lumi-R_L and R1 intermediates are almost unaffected. As in *Syn*Cph2(1-2), the lumi-R_L-like intermediate decays with a lifetime of 1.3 μs and exhibits an increase in absorbance in the long wavelength range at about 690 nm. This effect is continued in the second intermediate (R1, lifetime of 112 μs) that also displays a reduced absorbance at 620 nm. The highest impact on the absorbance change takes place during the formation of the R2 intermediate with a lifetime of 1.57 ms, also nearly two times faster than in native *Syn*Cph2(1-2). Here, a pronounced absorbance decrease around 655 nm takes place. The last intermediate, R3′, with a lifetime of 8.10 ms is distinct from the R3 intermediate of native *Syn*Cph2(1-2). Instead of an absorbance increase at 700 nm as detected for the native photosensor, the R3′ intermediate of the S385A mutant displays a broader increase above 590 nm with maximal changes at 660 nm. This spectral signature reflects the broad absorbance band of the P_{fr} form, as was seen before in steady state difference spectra.

The signals in the S385A measurements are 3-fold diminished compared with the native *Syn*Cph2(1-2) module not only during the $P_r \rightarrow P_{fr}$ but also the $P_{fr} \rightarrow P_r$ photoconversion. Like *Syn*Cph2(1-2), S385A shows three intermediates for the $P_{fr} \rightarrow P_r$ conversion, lumi-F′, F1, and F2 with lifetimes of 1.3 μs, 619 μs and 3.53 ms, which all exhibit the spectral signatures of a state close to P_r. The lumi-F′ intermediate is the only one that differs from lumi-F of intact *Syn*Cph2(1-2), because it displays an absorbance rise also at wavelengths above ~640 nm. The greatest absorbance changes occur during the formation of intermediate F2 with an absorbance rise at 640 nm. The lumi-F′ and F1 intermediates decay similarly as their *Syn*Cph2(1-2) counterparts; only the F2 intermediate decays nearly two times faster.

The *Syn*Cph2(1-2) mutant W389A addresses the role of the conserved W*X*E motif in the tongue region. This motif is about 15 Å distant from the bilin chromophore and is suggested as being part of a tryptophan switch during photoconversion (8). Like the S385A mutant, the W389A mutant shows a spectrum after red light illumination that lacks the signatures of the P_{fr} state (Fig. 1*B*). This alternative steady state spectrum is highly broadened with an unusual absorbance rise in the 450 – 600 nm region that surpasses the one of S385A. The P_r peak at 644 nm is bleached; the isosbestic point at 573 nm is red-shifted compared with S385A because of the broader absorbance. Global analysis of the time-resolved data reveals three instead of four intermediates (lumi-R_L, R1, and R2′) with lifetimes of 1.4 μs, 414 μs, and 2.28 ms (Fig. 3). Interestingly, these intermediates resemble the native intermediates not only in their lifetimes but also in the global features of their difference spectra. The first lumi-R-like intermediate with a lifetime of 1.4 μs shows an absorbance rise at 700 nm that is continued by the intermediate R1. The 2.28-ms R2′ intermediate exhibits an absorbance decrease not only in the range of *Syn*Cph2(1-2) (λ_{max} ~660 nm) but also at longer wavelengths, where intermediate R1 already shows signatures of the P_{fr} state. Unlike the wild type and the S385A mutant, this tongue mutant shows a pronounced rise of absorbance below 580 nm for the R2′ intermediate. A fourth

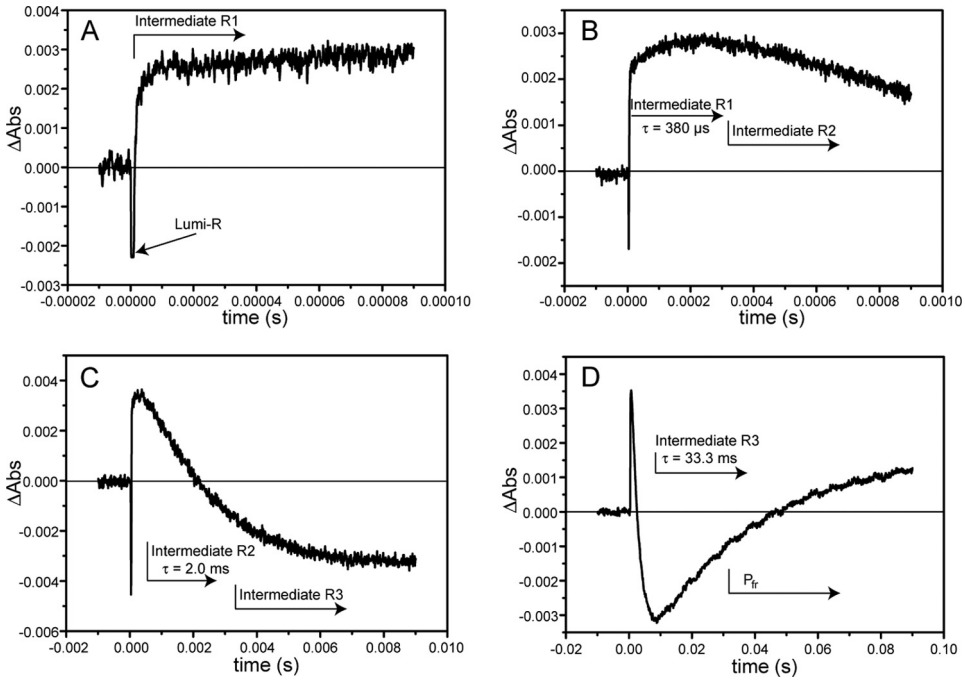

FIGURE 5. **Single time traces of the *Syn*Cph2(1-2) W389F $P_r \rightarrow P_{fr}$ transition measured at 665 nm.** *A–D* shows the single time traces with increasing time scales that are similar to *Syn*Cph2(1-2). The intermediates with their lifetimes are indicated by the *arrows*. The lifetimes were calculated via fitting of the single time traces and are averaged over the different observed wavelengths.

intermediate R3, as in *Syn*Cph2(1-2) and S385A, which is indicative of late conformational changes of the photoreceptor module, is missing. The signal intensities of the late R2′ intermediate and the final state of the W389A variant are again three to four times smaller than in *Syn*Cph2(1-2) and hence are in accordance with the S385A variant.

The $P_{fr} \rightarrow P_r$ back conversion of W389A reveals three intermediates (lumi-F″, F1′, and F2′) with lifetimes of 1.2 μs, 2.21 ms, and 19.5 ms. Although the intermediates already show the known P_r-like features, their LADS differ from native *Syn*Cph2(1-2) and its S385A mutant. Furthermore, the back reaction takes three times longer, and the constant difference spectrum (Fig. 3) corresponding to the final P_r conformation shows a comparatively broadened peak.

For the variant W389F with native *Syn*Cph2(1-2)-like steady state spectra, only a few wavelengths were measured to allow the prediction of the intermediates and their lifetimes. W389F behaves like *Syn*Cph2(1-2) in all observed wavelengths (Fig. 5) and reveals four observable intermediates in the forward reaction. The lifetimes of the intermediates calculated from the single time traces and not by global analysis are 1.5 μs, 380 μs, 2.0 ms, and 33.3 ms. The lifetimes of lumi-R_L, R1, and R2 are in good agreement with those of the native *Syn*Cph2(1-2) photosensor. Only the intermediate R3 differs in its lifetime that is two times longer than in *Syn*Cph2(1-2). In the reverse reaction only the lifetime of intermediate F2 could be assigned via fit of the single time traces. Without global analysis, the absorbance changes between the intermediates are too small to allow reliable fitting of the curves. The lifetime of intermediate F2 (3.1 ms) is two times faster than that of *Syn*Cph2(1-2).

DISCUSSION

Photoconversion of SynCph2(1-2), a PAS-less Phytochrome—Cyanobacterial phytochromes of group I (*e.g.* Cph1 and CphA) are well characterized with respect to their photochemical activity (5, 7, 18, 22, 23). In contrast, photoreceptors such as *Syn*Cph2(1-2), composed of only two GAF domains in a tandem array and lacking the N-terminal PAS domain, have not been investigated before by time-resolved spectroscopy. Despite the deviant domain arrangement, the tandem-GAF Cph2 photoreceptor highly resembles canonical phytochromes by undergoing a photochromic switch between a red-absorbing and a far red-absorbing state. Here, the photocycles of recombinant *Syn*Cph2(1-2) and three mutants within the PR*X*SF and W*X*E motif of the tongue region were characterized in the micro- to-millisecond time scale, which all share the primary $15Z \rightarrow 15E$ photochemistry. Following other studies on various phytochromes (18), we applied a sequential, unidirectional model for the generation and decay of intermediates. Even if equilibria between intermediates were involved, the final reaction products in these measurements will be the photostates, *i.e.* P_{fr} for the forward reaction or P_r, if the back conversion was followed. In this case, the kinetics and reaction rates that evolve from global fit analysis correspond to the ratios k_n/k_{-n}. For native *Syn*Cph2(1-2), three intermediates, R1 to R3, could be observed after lumi-R_L formation. While the decay time of 2.56 ms, assigned to intermediate R2, identifies the decay of short wavelength intermediates, the dominant contribution to P_{fr} formation is found for R3 with an observed lifetime of 17.1 ms.

In the canonical phytochromes from plants, the $P_r \rightarrow P_{fr}$ phototransformation was found to be extremely complex with

up to six intermediates (22), which can include a further series of P_{fr}-like states prior to the final formation of P_{fr}. For *Syn*Cph2(1-2) similar slow reactions cannot *per se* be excluded, because the reported late spectral changes were too red-shifted (>700 nm) to be in the range of this study. However, the absorbance properties of *Syn*Cph2(1-2) are blue-shifted compared with these canonical phytochromes (9).

It is intriguing to compare the detected absorbance changes for *Syn*Cph2(1-2) with those from group I phytochromes, especially in the pico- to microsecond time range. The excitation/detection setup as employed here yields a step function in the wavelength range of the first intermediate (around 700 nm), as "lumi-R" or I_{700} is formed within picoseconds (1) and remains constant far into the microsecond time range. The decay of this intermediate is described for group I phytochromes with a lifetime of ~80–100 μs (7, 23). In group I phytochromes, the following intermediates (meta-R or I_{bleach}) show reduced oscillator strength (I_{bleach}), and the decay of the first intermediate follows monoexponential kinetics. In Cph2, however, the absorbance around 700 nm, after being formed as a step function, remains positive over the entire time range of detection. Accordingly, one may assume that *Syn*Cph2(1-2) intermediates following the lumi-R-like state show a larger oscillator strength and thus do not cause a transient bleaching. For the reverse $P_{fr} \rightarrow P_r$ reaction, three intermediates, lumi-F, -F1, and -F2, are detected that all show the signatures of the P_r state and undergo only minor changes. These findings, especially the spectral similarity of all intermediates with the final photoproduct, P_r, are in accordance to the behavior of group I phytochromes. For comparison, laser flash photolysis studies of *Syn*Cph1 revealed five intermediates with time constants of at 4.5 μs, 270 μs, 3.8 ms, 30 ms, and 280 ms at pH 8.0 during the $P_r \rightarrow P_{fr}$ phototransformation (24). The fifth intermediate with a comparable long lifetime therefore cannot be found in *Syn*Cph2(1-2). Initial $Z \rightarrow E$ isomerization in *Syn*Cph1 occurs in the electronically excited P_r* state with a time constant of 30 ps according to an infrared spectroscopy analysis (25). A complementary Raman spectroscopy study concluded that 85% of the molecules relax back from the excited P_r* state to the P_r ground state explaining the low quantum yield of phytochrome phototransformation. After isomerization, the residual 15% were supposed to reach a product-like electronically excited Lumi-R* state that decays to the Lumi-R ground state, which is formed within 30 ps (26). Recent multipulse pump-probe data indicate that isomerization proceeds, most likely via a conventional conical intersection, between the excited and ground state energy surfaces (27). In any case, parts of the kinetic data of *Syn*Cph1 (5, 7, 24, 25, 28) combined with structural NMR data (29, 30) allow the assignment of structural changes to the various intermediates. Unfortunately, only the nearest chromophore environment in the chromophore-binding site was addressed, which excludes most of the tongue region, which is very similar in *Syn*Cph1 and *Syn*Cph2 (8).

Another cyanobacterial phytochrome of group I, the *Syn*Cph1 orthologue CphA from *Calothrix* sp. PCC7601 (also known as *Fremyella diplosiphon* or *Tolypothrix* sp.) revealed four intermediates with lifetimes of 8 μs, 330 μs, 3.2 ms, and 23 ms for the $P_r \rightarrow P_{fr}$ conversion and four intermediates with lifetimes of 1.5 μs, 1.5 ms, 6 ms, and 50 ms for the backward reaction (18). These results are again in good agreement with the *Syn*Cph2(1-2) lifetimes apart from the fourth intermediate of CphA in the $P_{fr} \rightarrow P_r$ photoconversion. Cryotrapping experiments of CphA in combination with UV-visible and Fourier transform infrared difference spectroscopy revealed the presence of three intermediates in the forward and two intermediates in the backward reaction that show remarkable similarities with the intermediates of *Syn*Cph1 (31).

The assignment of intermediates to structural changes can be achieved for at least two intermediates in the $P_r \rightarrow P_{fr}$ conversion (29). The lumi-R state is initially formed by double-bond $Z \rightarrow E$ isomerization between C15 and C16 (26, 32). In the meta-R state, the chromophore is transiently deprotonated at the D-ring nitrogen and is then reprotonated upon P_{fr} formation (24).

In *Syn*Cph2(1-2), the lumi-R state can be assigned to the first intermediate of this study. Because of its fast formation below the resolution limit of the measurements, only its decay can be followed. The remaining intermediates reflect structural changes in the protein as well as adaptations of the chromophore. The assignment of the transient protonation to the intermediates is not possible at the current state. Model compounds exhibit a red-shift upon protonation (33–35). For *Syn*Cph1, the transient proton release and a kinetic isotope effect were assigned to an intermediate with the 320-μs lifetime (7). Interestingly, its difference spectrum and lifetime resembles intermediate R1 of *Syn*Cph2(1-2); both exhibit a red-shifted absorbance.

The $P_{fr} \rightarrow P_r$ conversion starts like the forward reaction with the double bond isomerization between C15 and C16 leading to the lumi-F intermediate. Subsequent conformational changes in the range of rings C and D result in the formation of the intermediate meta-F. The meta-F $\rightarrow P_r$ transition is accompanied by the generation of a new hydrogen bond between the D-ring nitrogen and a water molecule (30).

Tongue Variants and Their Impact on the Photocycle—The tongue region of the GAF2 domain seals the chromophore binding pocket in GAF1 and is supposed to be involved in signal transduction (8, 36). This arrangement is comparable with the group I phytochromes where the tongue protrudes from the PHY domain, which is actually a degenerated GAF domain. Ser-385 is located in the PR*X*SF motif within a loop region of the tongue (Fig. 1*A*). The preceding residue Arg-383 of this motif is involved in the arginine to aspartate salt bridge, thereby generating a tight interaction between the GAF1 and GAF2 domain. Ser-385 points out of the binding pocket in the crystal structure of the P_r conformation, whereas Trp-389 is part of the conserved W*X*E motif in the stem region of the tongue consisting of two β-strands (Fig. 1*A*). Although Ser-385 and Trp-389 are ~13 and ~16 Å, respectively, apart from the D-ring of the chromophore in the P_r state, they affect formation of the P_{fr} state. Steady state absorbance spectra of their alanine variants reveal that they fail to form substantial amounts of a P_{fr} state like native *Syn*Cph2(1-2) (Fig. 1*B*).

In this study we could show that S385A exhibits four intermediates in the $P_r \rightarrow P_{fr}$ reaction like native *Syn*Cph2(1-2). Both share the first three intermediates lumi-R_L, -R1, and -R2 of

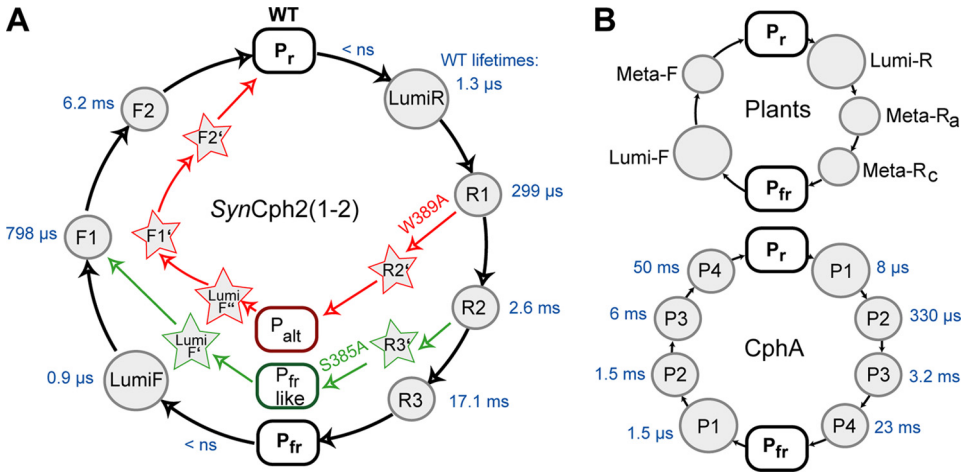

FIGURE 6. *A,* photocycle of the group II phytochrome *Syn*Cph2(1-2) (*black lines*) and its S385A (*green*) and W389A (*red*) mutants. *Rounded rectangles* highlight the ground state P_r and the P_{fr}- or P_{fr}-like states. *Circles* indicate the intermediates of the *Syn*Cph2(1-2) photocycle. The lifetimes of the wild type intermediates are shown next to them in *blue*. *Arrows* indicate deviations from the native photocycle as caused by mutations within the tongue region. The corresponding intermediates are depicted with *stars*. P_{alt} refers to an alternative red light-adapted state distinct from P_{fr}. *B,* photocycles of group I phytochromes. Only a minimal model is shown for the photocycle of plant phytochromes (*top*). The photocycle of CphA, another group I phytochrome, from the cyanobacterium *Calothrix* sp. PCC7601 (18) includes the lifetimes of the observed intermediates (*blue*) as obtained by a procedure comparable with *Syn*Cph2(1-2).

the $P_r \rightarrow P_{fr}$ reaction. The fourth intermediate R3′ differs in S385A (Fig. 3), but nevertheless, it decays to a P_{fr}-like state (Fig. 6). The $P_{fr} \rightarrow P_r$ conversion is very similar to *Syn*Cph2(1-2), suggesting that the red light adapted state of S385A decays into a comparable intermediate like the P_{fr} state of *Syn*Cph2(1-2) and that the P_{fr} and P_{fr}-like states correspond to each other. From this first intermediate lumi-F′, the protein decays via the common intermediates F1 and F2 of the *Syn*Cph2(1-2) $P_{fr} \rightarrow P_r$ photoconversion.

In contrast, the photocycle of the W389A variant at first glance differs from native *Syn*Cph2(1-2). The forward $P_r \rightarrow P_{fr}$ reaction proceeds through the first two *Syn*Cph2(1-2)-like intermediates lumi-R_L and -R1. The third intermediate R2′ deviates and decays without a fourth intermediate like in *Syn*Cph2(1-2) to the red light-adapted state that shows a very broad absorbance band, including an absorbance rise around 550 nm (Fig. 1*B*, *bottom, left panel*). This state represents an alternative photoproduct and is therefore named here P_{alt}. W389A apparently misses the last intermediate R3 (Fig. 3, *panel bottom, left panel*), although a meta-R-like decay with a lifetime of ~2.3 ms (akin those of the wild type and the S385A mutant) can clearly be identified. The inspection of the steady state P_r/P_{fr} difference spectrum of this mutant (Fig. 1*B*, *bottom, left panel*) clarifies this confusion, as it shows a red light-adapted state with an apparently small oscillator strength that cannot be detected in the lifetime-associated difference spectrum. Interestingly, any conversion processes of intermediates of the entire detection range are covered from the contributions of the very broad absorbance of the P_{alt} form.

The difference between the red light-adapted states of S385A and W389A is also reflected by their circular dichroism (CD) spectra. Here, W389A shows increased ellipticity at 550 nm, whereas S385A exhibits only a smaller effect and corresponds to *Syn*Cph2(1-2) (8). Interestingly, the W389A steady state absorbance difference spectrum corresponds to that of the *Syn*Cph2(1) fragment that consists only of the GAF1 domain and therefore lacks the tongue region altogether (37). The difference spectrum of W389A also resembles that of a 45-kDa fragment (amino acids 1–425) of the plantal phytochrome A from *Avena sativa.* This recombinant PhyA fragment was designed to study the properties of the proteolytic 39-kDa fragment of PhyA of *A. sativa*; however, trypsin digestion of the native protein also causes loss of the N-terminal 65 amino acids. Accordingly, this PhyA fragment that lacks most of the PHY domain forms upon irradiation a red light-adapted state (38) with a very broad absorbance band at 550 nm and only moderate thermal stability, thus phenomenologically indicating the importance of the PHY domain and its tongue region. The spectral similarity between phytochrome fragments, which either lack their second GAF/PHY domain or bear disruptive mutations within their PR*X*SF motif like R383D (9) and the W389A mutant of *Syn*Cph2(1-2), now clearly highlights the role of the tryptophan in the W*X*E motif for tongue rearrangement and stability of the P_{fr} form. Accordingly, W389A undergoes three intermediates in the back reaction to P_r that differ significantly from the intermediates of *Syn*Cph2(1-2) (Fig. 6), and the overall time elapsed to arrive at the P_r state is three times longer than for *Syn*Cph2(1-2) (19.5 *versus* 6.20 ms, *cf.* Table 1).

From these findings, one can conclude that although the Ser-385 residue contributes to a native-like P_{fr} formation, it is not essential for the formation of the first three intermediates of the $P_r \rightarrow P_{fr}$ reaction and the intermediate two and three of the $P_{fr} \rightarrow P_r$ photoconversion. Only the formation of the final $P_r \rightarrow P_{fr}$ intermediate R3 and of lumi-F is affected by this serine. Accordingly, the S385A variant shows the same conformational changes at the chromophore level during photoconversion and only slight differences at the late stages of the protein environment's adjustment, *i.e.* the steps leading to and from P_{fr}, as compared with *Syn*Cph2(1-2). Interestingly, Ser-385 apparently stabilizes the intermediates because its alanine mutation exhibits about 5-fold faster photoconversions.

The alanine mutation of Trp-389, however, shows major implications on the photocycle; it only shares the first two intermediates with *Syn*Cph2(1-2). This suggests that this amino acid

plays a key role in the structural rearrangements during the late photoconversion. Interestingly, the phenylalanine mutation suffices to restore the native *Syn*Cph2(1-2) behavior.

Mutagenesis studies in the photosensory module of oat phytochrome A (39) with amino acids in close proximity to the chromophore in the GAF domain revealed different effects on the decay of I_{700} (lumi-R). Some mutants displayed faster decays and accelerated P_{fr} formation, whereas a proline to alanine mutation resulted in a slower P_{fr} formation due to a more rigid conformation in the mutant. The acceleration was assigned to an increase in polarity or a weakened interaction between two protein domains enabling faster conformational changes (39). In *Syn*Cph2(1-2), the S385A mutation accelerated the formation of the red light-adapted state, where the decrease of polarity inhibits interactions that stabilize the intermediates. W389F shows a slower P_{fr} formation due to the less bulky amino acid substitute that is crucial to allow formation of the new tongue conformation.

Lessons from the Photocycle, a Tryptophan Switch for Signaling—We previously suggested a conformational change during photoconversion that involves a tryptophan switch of residues in the tongue region (8). We suggested the tryptophan residues of the W(G/A)G and W*X*E motif act as anchors within the structure for stabilizing either the P_r or the P_{fr} state. It can be concluded that bulky aromatic residues like phenylalanine can substitute the function of tryptophan and preserve the *Syn*Cph2(1-2) behavior, whereas small residues such as alanine fail to do so.

In this study, we demonstrate that the W389A variant has indeed major implications on the photocycle in comparison with S385A. On their way to the red light-adapted state, the alanine mutation of the former prevents structural changes important for P_{fr} formation. Assuming that these structural changes imply rearrangements of the tongue, one can postulate that W389A forms a "miss-docked" and S385A a "well docked" tongue after red light illumination. The fact that S385A has a smaller effect on the photocycle and does not further affect P_{fr} formation demonstrates that only tryptophans provide contributions crucial to the photoconversion. The *Syn*Cph2(1-2) like behavior of W389F shows that a bulky and/or aromatic character is important for the function of the switch. Interestingly, only the lifetime of the final intermediate R3 in the W389F photocycle differs from *Syn*Cph2(1-2). Its lifetime is 2-fold longer than its wild type counterpart, which is apparently caused by the smaller amino acid and the higher intrinsic flexibility. The alanine mutation already affects intermediate R2. This suggests that the intermediates lumi-R_L and R1 reflect only changes in the chromophore and its nearest environment, whereas in the intermediate R2 large scale changes in the tongue region occur, and a big aromatic amino acid in the Trp-389 position is needed to complete this process. The difference between phenylalanine and tryptophan in this position affects only the last intermediate R3. The S385A variant shows that the involvement of the serine in the interactions occurs later than that of the tryptophan residue in intermediate R3. In bathyphytochrome structures, which correspond to their P_{fr} ground state, this serine points toward the chromophore in contrast to P_r structures and is there involved in an extended hydrogen bond network, including the pyrrole nitrogen of ring D. Our results suggest that a movement of the serine residue of the PR*X*SF motif and hence the formation of the hydrogen bond network occurs during the formation of intermediate R3.

During $P_{fr} \rightarrow P_r$ photoconversion, the S385A mutation only affects lumi-F, whereas photoconversion of W389A proceeds via a different set of intermediates. The implications of the mutations on the back reaction are not as big as in the forward reaction, because in lumi-F the protein already shows P_r-like characteristics and the following intermediates reflect only minor changes. This finding again demonstrates the paramount importance of the tryptophan residues in the Trp switch for the P_{fr} formation of phytochromes.

Acknowledgments—We thank Norbert Dickmann and Petra Gnau for technical assistance.

REFERENCES

1. Andel, F., Hasson, K. C., Gai, F., Anfinrud, P. A., and Mathies, R. A. (1997) Femtosecond time-resolved spectroscopy of the primary photochemistry of phytochrome. *Biospectroscopy* **3,** 421–433
2. Jorissen, H. J., Quest, B., Remberg, A., Coursin, T., Braslavsky, S. E., Schaffner, K., de Marsac, N. T., and Gärtner, W. (2002) Two independent, light-sensing two-component systems in a filamentous cyanobacterium. *Eur. J. Biochem.* **269,** 2662–2671
3. Müller, M. G., Lindner, I., Martin, I., Gärtner, W., and Holzwarth, A. R. (2008) Femtosecond kinetics of photoconversion of the higher plant photoreceptor phytochrome carrying native and modified chromophores. *Biophys. J.* **94,** 4370–4382
4. Bischoff, M., Hermann, G., Rentsch, S., and Strehlow, D. (2001) First steps in the phytochrome phototransformation: a comparative femtosecond study on the forward (Pr → Pfr) and back reaction (Pfr → Pr). *Biochemistry* **40,** 181–186
5. Heyne, K., Herbst, J., Stehlik, D., Esteban, B., Lamparter, T., Hughes, J., and Diller, R. (2002) Ultrafast dynamics of phytochrome from the cyanobacterium *Synechocystis*, reconstituted with phycocyanobilin and phycoerythrobilin. *Biophys. J.* **82,** 1004–1016
6. Michler, I., and Braslavsky, S. E. (2001) Time-resolved thermodynamic analysis of the oat phytochrome A phototransformation. A photothermal beam deflection study. *Photochem. Photobiol.* **74,** 624–635
7. Remberg, A., Lindner, I., Lamparter, T., Hughes, J., Kneip, C., Hildebrandt, P., Braslavsky, S. E., Gärtner, W., and Schaffner, K. (1997) Raman spectroscopic and light-induced kinetic characterization of a recombinant phytochrome of the cyanobacterium *Synechocystis*. *Biochemistry* **36,** 13389–13395
8. Anders, K., Daminelli-Widany, G., Mroginski, M. A., von Stetten, D., and Essen, L.-O. (2013) Structure of the cyanobacterial phytochrome 2 photosensor implies a tryptophan switch for phytochrome signaling. *J. Biol. Chem.* **288,** 35714–35725
9. Anders, K., von Stetten, D., Mailliet, J., Kiontke, S., Sineshchekov, V. A., Hildebrandt, P., Hughes, J., and Essen, L.-O. (2011) Spectroscopic and photochemical characterization of the red-light sensitive photosensory module of Cph2 from *Synechocystis* PCC 6803. *Photochem. Photobiol.* **87,** 160–173
10. Rockwell, N. C., and Lagarias, J. C. (2010) A brief history of phytochromes. *Chem. Phys. Chem.* **11,** 1172–1180
11. Montgomery, B. L., and Lagarias, J. C. (2002) Phytochrome ancestry: sensors of bilins and light. *Trends Plant Sci.* **7,** 357–366
12. Savakis, P., De Causmaecker, S., Angerer, V., Ruppert, U., Anders, K., Essen, L.-O., and Wilde, A. (2012) Light-induced alteration of c-di-GMP level controls motility of *Synechocystis* sp. PCC 6803. *Mol. Microbiol.* **85,** 239–251
13. Simm, R., Morr, M., Kader, A., Nimtz, M., and Römling, U. (2004) GGDEF and EAL domains inversely regulate cyclic di-GMP levels and transition

from sessility to motility. *Mol. Microbiol.* **53,** 1123–1134
14. Takala, H., Björling, A., Berntsson, O., Lehtivuori, H., Niebling, S., Hoernke, M., Kosheleva, I., Henning, R., Menzel, A., Ihalainen, J. A., and Westenhoff, S. (2014) Signal amplification and transduction in phytochrome photosensors. *Nature* **509,** 245–248
15. Chizhov, I., Chernavskii, D. S., Engelhard, M., Mueller, K. H., Zubov, B. V., and Hess, B. (1996) Spectrally silent transitions in the bacteriorhodopsin photocycle. *Biophys. J.* **71,** 2329–2345
16. Chizhov, I., and Engelhard, M. (2001) Temperature and halide dependence of the photocycle of halorhodopsin from *Natronobacterium pharaonis*. *Biophys. J.* **81,** 1600–1612
17. Chizhov, I., Schmies, G., Seidel, R., Sydor, J. R., Lüttenberg, B., and Engelhard, M. (1998) The photophobic receptor from *Natronobacterium pharaonis*: temperature and pH dependencies of the photocycle of sensory rhodopsin. *Biophys. J.* **75,** 999–1009
18. Chizhov, I., Zorn, B., Manstein, D. J., and Gärtner, W. (2013) Kinetic and thermodynamic analysis of the light-induced processes in plant and cyanobacterial phytochromes. *Biophys. J.* **105,** 2210–2220
19. Zhao, K. H., Ran, Y., Li, M., Sun, Y. N., Zhou, M., Storf, M., Kupka, M., Böhm, S., Bubenzer, C., and Scheer, H. (2004) Photochromic biliproteins from the cyanobacterium *Anabaena* sp. PCC 7120: lyase activities, chromophore exchange, and photochromism in phytochrome AphA. *Biochemistry* **43,** 11576–11588
20. Brandlmeier, T., Scheer, H., and Rüdiger, W. (1981) Chromophore content and molar absorptivity of phytochrome in the Pr-form. *Z. Naturforsch.* **36c,** 431–439
21. Ishizuka, T., Narikawa, R., Kohchi, T., Katayama, M., and Ikeuchi, M. (2007) Cyanobacteriochrome TePixJ of *Thermosynechococcus elongatus* harbors phycoviolobilin as a chromophore. *Plant Cell Physiol.* **48,** 1385–1390
22. Schmidt, P., Gertsch, T., Remberg, A., Gärtner, W., Braslavsky, S. E., and Schaffner, K. (1998) The complexity of the Pr to Pfr phototransformation kinetics is an intrinsic property of native phytochrome. *Photochem. Photobiol.* **68,** 754–761
23. Remberg, A., Ruddat, A., Braslavsky, S. E., Gärtner, W., and Schaffner, K. (1998) Chromophore incorporation, Pr to Pfr kinetics, and Pfr thermal reversion of recombinant N-terminal fragments of phytochrome A and B chromoproteins. *Biochemistry* **37,** 9983–9990
24. van Thor, J. J., Borucki, B., Crielaard, W., Otto, H., Lamparter, T., Hughes, J., Hellingwerf, K. J., and Heyn, M. P. (2001) Light-induced proton release and proton uptake reactions in the cyanobacterial phytochrome Cph1. *Biochemistry* **40,** 11460–11471
25. Yang, Y., Linke, M., von Haimberger, T., Hahn, J., Matute, R., González, L., Schmieder, P., and Heyne, K. (2012) Real-time tracking of phytochrome's orientational changes during Pr photoisomerization. *J. Am. Chem. Soc.* **134,** 1408–1411
26. Dasgupta, J., Frontiera, R. R., Taylor, K. C., Lagarias, J. C., and Mathies, R. A. (2009) Ultrafast excited-state isomerization in phytochrome revealed by femtosecond stimulated Raman spectroscopy. *Proc. Natl. Acad. Sci. U.S.A.* **106,** 1784–1789
27. Kim, P. W., Rockwell, N. C., Freer, L. H., Chang, C.-W., Martin, S. S., Lagarias, J. C., and Larsen, D. S. (2013) Unraveling the primary isomerization dynamics in cyanobacterial phytochrome Cph1 with multipulse manipulations. *J. Phys. Chem. Lett.* **4,** 2605–2609
28. Heyes, D. J., Khara, B., Sakuma, M., Hardman, S. J., O'Cualain, R., Rigby, S. E., and Scrutton, N. S. (2012) Ultrafast red light activation of *Synechocystis* phytochrome Cph1 triggers major structural change to form the Pfr signalling-competent state. *PLoS One* **7,** e52418
29. Song, C., Rohmer, T., Tiersch, M., Zaanen, J., Hughes, J., and Matysik, J. (2013) Solid-state NMR spectroscopy to probe photoactivation in canonical phytochromes. *Photochem. Photobiol.* **89,** 259–273
30. Rohmer, T., Lang, C., Bongards, C., Gupta, K. B., Neugebauer, J., Hughes, J., Gärtner, W., and Matysik, J. (2010) Phytochrome as molecular machine: revealing chromophore action during the Pfr → Pr photoconversion by magic-angle spinning NMR spectroscopy. *J. Am. Chem. Soc.* **132,** 4431–4437
31. Schwinté, P., Gärtner, W., Sharda, S., Mroginski, M.-A., Hildebrandt, P., and Siebert, F. (2009) The photoreactions of recombinant phytochrome CphA from the cyanobacterium *Calothrix* PCC7601: a low-temperature UV-Vis and FTIR study. *Photochem. Photobiol.* **85,** 239–249
32. Andel, F., 3rd., Lagarias, J. C., and Mathies, R. A. (1996) Resonance raman analysis of chromophore structure in the Lumi-R photoproduct of phytochrome. *Biochemistry* **35,** 15997–16008
33. Borucki, B. (2006) Proton transfer in the photoreceptors phytochrome and photoactive yellow protein. *Photochem. Photobiol. Sci.* **5,** 553–566
34. Margulies, L., and Stockburger, M. (1979) Spectroscopic studies on model compounds of the phytochrome chromophore. Protonation and deprotonation of biliverdin dimethyl ester. *J. Am. Chem. Soc.* **101,** 743–744
35. Stanek, M., and Grubmayr, K. (1998) Protonated 2,3-dihydrobilindiones—models for the chromophores of phycocyanin and the red-absorbing form of phytochrome. *Chem. Eur. J.* **4,** 1653–1659
36. Essen, L. O., Mailliet, J., and Hughes, J. (2008) The structure of a complete phytochrome sensory module in the Pr ground state. *Proc. Natl. Acad. Sci. U.S.A.* **105,** 14709–14714
37. Wu, S. H., and Lagarias, J. C. (2000) Defining the bilin lyase domain: lessons from the extended phytochrome superfamily. *Biochemistry* **39,** 13487–13495
38. Gärtner, W., Hill, C., Worm, K., Braslavsky, S. E., and Schaffner, K. (1996) Influence of expression system on chromophore binding and preservation of spectral properties in recombinant phytochrome A. *Eur. J. Biochem.* **236,** 978–983
39. Remberg, A., Schmidt, P., Braslavsky, S. E., Gärtner, W., and Schaffner, K. (1999) Differential effects of mutations in the chromophore pocket of recombinant phytochrome on chromoprotein assembly and Pr-to-Pfr photoconversion. *Eur. J. Biochem.* **266,** 201–208